Accounting for ground motion uncertainty in empirical seismic fragility modeling

Lukas Bodenmann *[1], Jack Baker[2], and Božidar Stojadinović[1]

[1]Department of Civil, Environmental and Geomatic Engineering, ETH Zurich
[2]Department of Civil and Environmental Engineering, Stanford University

November 2023

ABSTRACT

Seismic fragility models provide a probabilistic relation between ground motion intensity and damage, making them a crucial component of many regional risk assessments. Estimating such models from damage data gathered after past earthquakes is challenging because of uncertainty in the ground motion intensity the structures were subjected to. Here, we develop a Bayesian estimation procedure that performs joint inference over ground motion intensity and fragility model parameters. When applied to simulated damage data, the proposed method can recover the data-generating fragility functions, while the traditionally used method, employing fixed, best-estimate, intensity values, fails to do so. Analyses using synthetic data with known properties show that the traditional method results in flatter fragility functions that overestimate damage probabilities for low-intensity values and underestimate probabilities for large values. Similar trends are observed when comparing both methods on real damage data. The results suggest that neglecting ground motion uncertainty manifests in apparent dispersion in the estimated fragility functions. This undesirable feature can be mitigated through the proposed Bayesian procedure.

*Corresponding author: bodenmann (at) ibk.baug.ethz.ch

INTRODUCTION

Procedures for earthquake risk assessments often rely on probabilistic relations between ground shaking intensity and physical damage to elements of the built environment. A fragility function plots the probability of reaching or exceeding a certain damage limit state for increasing ground motion intensity measure (IM) levels. The fragility function parameters are derived from expert opinion (e.g., Rojahn and Sharpe, 1985), or estimated from data that is either generated through structural analyses of building archetypes, the so-called mechanical or analytical approach (e.g., Mosalam et al., 1997), or gathered after an earthquake event, the so-called empirical approach (e.g., Basöz and Kiremidjian, 1998).

Besides challenges in quality and coverage of post-earthquake damage surveys, empirical fragility modeling also requires assumptions on the IM values that caused the observed damage (Rossetto and Ioannou, 2018). These values are only known at locations of seismic network stations, and are uncertain at other locations. Thus, if a group of damaged buildings is observed, we do not know *a-priori* whether they were damaged because they were particularly vulnerable, because the ground shaking was particularly strong, or because of both. This study aims to provide further insights into this causality dilemma and proposes a new methodology to estimate fragility function parameters.

One common approach to address this causality dilemma assumes fixed, best-estimate, IM values for parameter estimation (Rossetto et al., 2014). The fixed values represent best-estimates that are typically chosen as the median of the IM distribution conditional on available data from seismic network stations (e.g., from a shake map). This fixed IM approach served as the basis for the vast majority of available empirical fragility functions, including early (e.g., Basöz and Kiremidjian, 1998) and recent studies (e.g., Rosti et al., 2021). By considering fixed IM values, such an approach does not account for potential deviations of the actual IM from this best-estimate. The sensitivity of estimated fragility function parameters with respect to IM uncertainty was examined by Ioannou et al. (2015) through simulated case studies. They found that unrealistically dense seismic networks are required to recover the "true" fragility parameters used to generate the data. For realistic network configurations, however, the approach based on fixed IM values led to substantial differences between estimated and "true" parameters. Approaches to account for IM uncertainty vary in the existing literature. For example, King et al. (2005) focused on damage survey data collected within a limited distance to a seismic network station. Lallemant et al. (2015) suggested weighting the observations according to the inverse of the remaining IM variance, thus assigning higher weight to data collected close to stations. Ioannou et al. (2015) simulated numerous IM values at the survey locations and performed parameter estimation for each simulation run. The resulting set of estimated parameters was then assumed to reflect IM uncertainty.

While aiming to account for IM uncertainty, the above approaches miss a crucial component of the causality dilemma, which is best explained by considering the inverse problem, where the true fragility function parameters are available. In this hypothetical case, studied by Pozzi and Wang (2018), the damage observations serve as noisy measurements of the uncertain IM values. Consequently, these observations can be used to obtain a constrained estimate of the IM values that caused the damage.

In cases of practical interest, both the fragility parameters and the IM values are uncertain. This study presents a Bayesian approach to estimate their joint posterior distribution, which can account for uncertainty in both the IM values and the fragility parameters. We start with an overview of fragility function definitions, followed by mathematical descriptions of the proposed Bayesian parameter estimation approach and the traditional, fixed IM, approach. Both methods are first explained on a simplified example and then compared using data from the 2009 L'Aquila (Italy) earthquake.

FRAGILITY FUNCTIONS

Empirical fragility modeling aims to estimate the fragility function parameters using observed or estimated values of IMs and building damage states. Damage states are obtained from post-earthquake building inspections, where experts describe the building characteristics and the sustained damage based on pre-specified guidelines and data-recording forms. Information on the building characteristics pertain to the material and the type of the load resisting system, as well as geometrical attributes such as the number of storeys. Buildings with similar characteristics are grouped into a 'building class' with a corresponding set of fragility functions. Damage descriptions are commonly reduced to ordered, collectively exhaustive and mutually exclusive damage states (e.g., no, slight, moderate, heavy and complete damage), which are numerically encoded as $ds \in \{0, 1, ..., c\}$. To ease the notation in the following definitions, we consider a single building class and assume that all damage observations for buildings of that class are treated equally.

The log-normal cumulative distribution is the most common functional form for fragility functions

$$\mathrm{P}(DS \geq ds|im) = \Phi\left(\frac{\ln(im/\theta_{ds})}{\beta_{ds}}\right) = \Phi\left(\frac{\ln im - \ln\theta_{ds}}{\beta_{ds}}\right) \ , \tag{1}$$

where $\Phi(\cdot)$ is the standard normal cumulative distribution function, θ_{ds} denotes the median IM which causes the structure to reach or exceed ds, and β_{ds} is the standard deviation of the $\ln IM$, here referred to as the dispersion parameter. From the fragility functions, one obtains the probability mass function, $\mathrm{P}(DS = ds|im) = p(ds|im)$, as

$$p(ds|im) = \begin{cases} 1 - \mathrm{P}(DS \geq ds+1|im), & \text{if } ds = 0 \\ \mathrm{P}(DS \geq ds|im), & \text{if } ds = c \\ \mathrm{P}(DS \geq ds|im) - \mathrm{P}(DS \geq ds+1|im), & \text{otherwise} \ . \end{cases} \tag{2}$$

To prevent negative probabilities in Eq. (2), we assume an identical dispersion parameter β for all damage states. This avoids a crossing of the fragility functions and is a standard assumption taken in analytical and empirical fragility modeling for ordered damage states (e.g., Martins and Silva, 2020; Rosti et al., 2021). For $c+1$ damage states, we thus have c increasing parameters $\theta_1 < \theta_2 < \cdots < \theta_c$ and one common dispersion parameter β.

A second fragility function definition, equivalent to Eq. (1), is obtained from the cumulative probit model (Lallemant et al., 2015). By introducing the threshold parameters $\eta_{ds} = \beta^{-1} \ln \theta_{ds}$, this alternative definition reads as

$$\mathrm{P}(DS \geq ds|im) = \Phi\left(\beta^{-1} \ln im - \eta_{ds}\right) \ . \tag{3}$$

Following Nguyen and Lallemant (2022), we use the re-parametrized definition of Eq. (3) with the transformed parameters η_{ds} still being of increasing order. To account for this ordering in the estimation algorithms, we introduce positive parameters $\delta_{ds} = \eta_{ds} - \eta_{ds-1}$ for states $ds > 1$. The parameters of interest are collectively denoted as vector $\boldsymbol{\vartheta} = [\beta, \eta_1, \delta_2, \ldots, \delta_c]^\top$. Finally, we denote the fragility model in terms of the probability mass function $p(ds|im, \boldsymbol{\vartheta})$, where we explicitly condition on parameter vector $\boldsymbol{\vartheta}$.

The use of log-normal fragility functions – leading to the cumulative probit model – dates back to earthquake risk assessments of critical infrastructure components (e.g., Kennedy et al., 1980) and is well-established in disaster risk analysis (e.g., Kircher et al., 1997) as well as in performance-based earthquake engineering (e.g., Porter et al., 2007). Yet, the herein presented estimation algorithms can also be used for alternative models, such as the cumulative logistic model employed by Basöz and Kiremidjian (1998).

ESTIMATING FRAGILITY FUNCTION PARAMETERS

Figure 1 depicts the probabilistic model relating the variables involved in the estimation of $\boldsymbol{\vartheta}$ by considering a damage data set from n buildings gathered after an earthquake with rupture characteristics **rup**. The fragility model of Eq. (2) relates the observed damage states, $\mathbf{ds} = [ds_i, \ldots, ds_n]^\top$, to the IM values at the locations of the surveyed buildings, $\mathbf{im}_\mathcal{B} = [im_1, \ldots, im_n]^\top$. Knowing the latter would allow estimating $\boldsymbol{\vartheta}$ with similar techniques used in analytical fragility modeling (e.g., Baker, 2015). In most cases, however, we only know the IM values at the locations of seismic stations, here denoted as $\mathbf{im}_\mathcal{S} = [im_{n+1}, \ldots, im_{n+m}]^\top$ for the case of m stations, while their counterparts at the survey locations are uncertain.

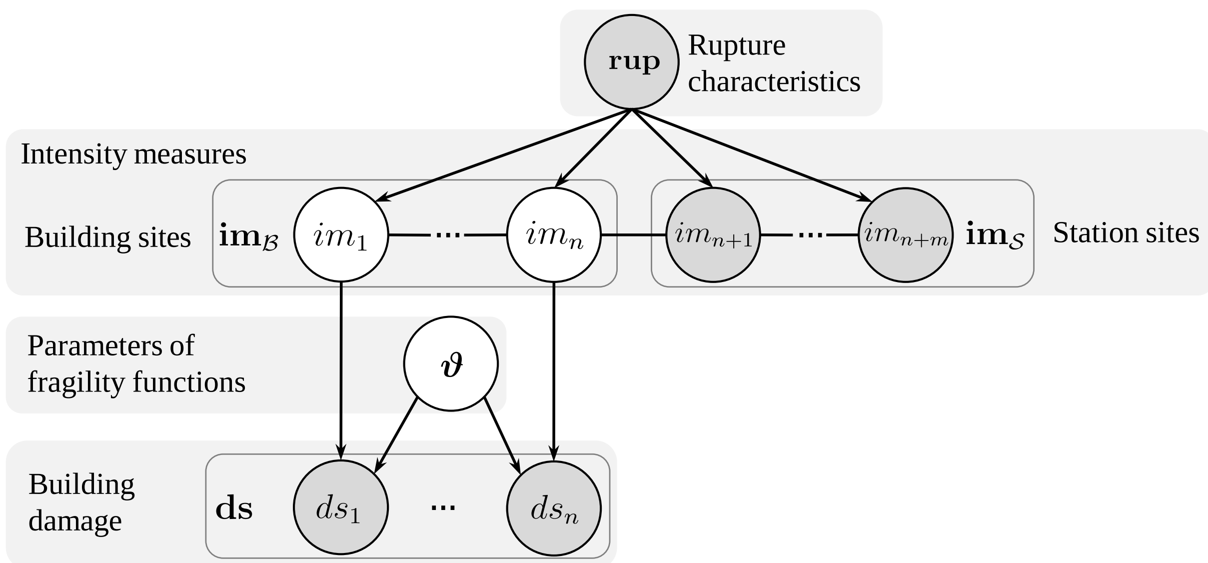

Figure 1: Probabilistic model to estimate fragility function parameters using data from building damage surveys and seismic network stations. Observed and unobserved variables are indicated with gray and white circles, respectively. The arrows indicate directed relationships between the variables. The horizontal lines illustrate that the intensity measures follow a joint multivariate distribution.

To constrain the above-mentioned uncertainty, we evaluate the distribution of $\mathbf{im}_\mathcal{B}$ conditional on station data $\mathbf{im}_\mathcal{S}$ and rupture characteristics **rup** by following Engler et al. (2022), who present the mathematical background for the most recent version of the United States Geology Survey's shake map system. Conditional on $\mathbf{rup}$ only, the joint distribution of $\mathbf{im}_\mathcal{B}$ and $\mathbf{im}_\mathcal{S}$ is assumed to be multivariate log-normal (Jayaram and Baker, 2008), with parameters derived from empirical ground motion models (GMMs) and spatial correlation models. Thus, the conditional distribution of interest also follows a multivariate log-normal distribution, i.e., $p(\mathbf{im}_\mathcal{B}|\mathbf{im}_\mathcal{S}, \mathbf{rup}) = \mathcal{LN}(\boldsymbol{\mu}_{\mathcal{B}|\mathcal{S}}, \boldsymbol{\Sigma}_{\mathcal{BB}|\mathcal{S}})$. The distributional parameters, $\boldsymbol{\mu}_{\mathcal{B}|\mathcal{S}}$ and $\boldsymbol{\Sigma}_{\mathcal{BB}|\mathcal{S}}$ are computed via Equations 4 and 5 in Engler et al. (2022), also explained in Appendix A of this study.

We next present two methodologies to estimate $\boldsymbol{\vartheta}$. The first, traditional, method assumes fixed – or deterministic – values for $\mathbf{im}_\mathcal{B}$. The second, proposed, method, treats both, $\boldsymbol{\vartheta}$ and $\mathbf{im}_\mathcal{B}$, as uncertain and follows a Bayesian approach for inference.

Maximum likelihood inference with fixed IM values

This estimation method replaces uncertain *IM* values at the survey sites with fixed, best-estimate, values derived from the conditional distribution $p(\mathbf{im}_\mathcal{B}|\mathbf{im}_\mathcal{S}, \mathbf{rup})$. For site i, the best-estimate value corresponds to $\widehat{im}_i = \exp([\boldsymbol{\mu}_{\mathcal{B}|\mathcal{S}}]_i)$, which is the median *IM* conditional on station data $\mathbf{im}_\mathcal{S}$. As depicted in Figure 1, the joint distribution of building damage conditional on the *IM* values at the building locations factorizes, i.e., $p(\mathbf{ds}|\mathbf{im}_\mathcal{B}, \boldsymbol{\vartheta}) = \prod_{i=1}^{n} p(ds_i|im_i, \boldsymbol{\vartheta})$. Assuming fixed *IM* values thus offers the advantage that the damage observations of different buildings can be treated independently, which makes it an efficient approach for large amounts of data. The parameters are then estimated by maximizing the log-likelihood

$$\hat{\boldsymbol{\vartheta}} = \underset{\boldsymbol{\vartheta}}{\operatorname{argmax}} \sum_{i=1}^{n} \ln p(ds_i|\widehat{im}_i, \boldsymbol{\vartheta}) \ , \tag{4}$$

such that the obtained parameter estimates maximize the probability of observing the surveyed damage under the chosen best-estimate *IM* values. In the following, we refer to this estimation method as the fixed IM approach.

Figure 2 illustrates a one dimensional example with simulated IM observations and damage data from two stations and 500 buildings resulting from a magnitude 6 earthquake with an epicenter at $x = 0$ km. The assumed fragility parameter values are 0.65, 0.2g, and 0.65g for β, θ_1 and θ_2, respectively, and the estimated values are 0.92, 0.25g, and 0.80g. From Figure 2b, we observe the substantial uncertainty around the median of $p(\mathbf{im}_{\mathcal{B}}|\mathbf{im}_{\mathcal{S}}, \mathbf{rup})$. By considering fixed IM values, this approach does not account for deviations of the "true" IM from this best-estimate. The estimated fragility functions, shown in Figure 2c, are flatter than the "true" functions used to generate the data. Such behavior was also observed in the simulated case studies by Ioannou et al. (2015) mentioned in the Introduction, and results from an overestimation of the dispersion parameter β. This overestimation indicates that IM uncertainty manifests as apparent uncertainty – or dispersion – in the fragility functions.

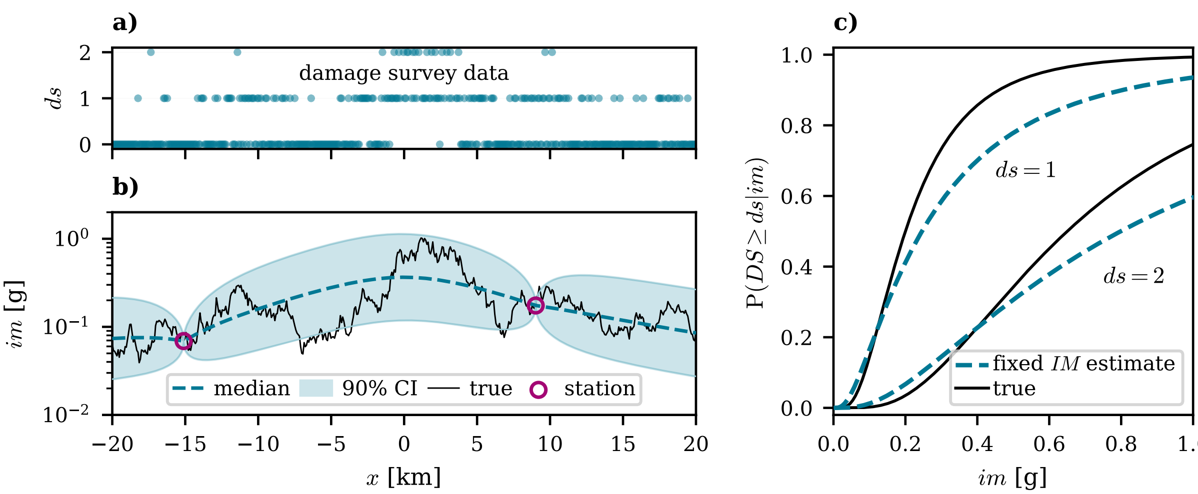

Figure 2: Fragility results from a one-dimensional example with simulated damage survey data. (a) Building damage states plotted versus their location. Damage states are simulated using the assumed "true" fragilities and IM values. (b) Simulated "true" IM values, with circles denoting the locations and IM values for two recording stations. The dashed line indicates the predicted median IM values and the shaded interval indicates the 90% credibility interval (CI) of the distribution conditional on data from the two stations. (c) The "true" fragility functions and the ones estimated with the fixed IM approach.

Bayesian inference with uncertain IM values

To account for ground motion uncertainty, we take a Bayesian approach treating both the fragility function parameters, $\boldsymbol{\vartheta}$, and the IM values at the survey sites, $\mathbf{im}_{\mathcal{B}}$, as realizations of random variables. The model shown in Figure 1 serves as the prior generative model which gives rise to the observed data. Based on this model, we express the joint posterior distribution of $\mathbf{im}_{\mathcal{B}}$ and $\boldsymbol{\vartheta}$ conditional on the triplet of damage survey data, $\mathbf{ds}$, station data, $\mathbf{im}_{\mathcal{S}}$, and rupture characteristics, $\mathbf{rup}$, as

$$p(\boldsymbol{\vartheta}, \mathbf{im}_{\mathcal{B}}|\mathbf{ds}, \mathbf{im}_{\mathcal{S}}, \mathbf{rup}) = \left(\prod_{i=1}^{n} p(ds_i|im_i, \boldsymbol{\vartheta})\right) \frac{p(\mathbf{im}_{\mathcal{B}}|\mathbf{im}_{\mathcal{S}}, \mathbf{rup})p(\boldsymbol{\vartheta})}{p(\mathbf{ds}|\mathbf{im}_{\mathcal{S}}, \mathbf{rup})}\ , \tag{5}$$

where the denominator, $p(\mathbf{ds}|\mathbf{im}_{\mathcal{S}}, \mathbf{rup})$, is the marginal likelihood, i.e., the probability that the prior model assigns to the observed damage data conditional on station data and rupture characteristics, and $p(\boldsymbol{\vartheta})$ is the prior distribution of the fragility function parameters. For each parameter we assign weakly informative priors, stated in Table 1, and assume that the parameters are *a-priori* independent. These distributions are chosen such that the resulting fragility functions provide sufficient adaptability to cover building classes with varying susceptibility to earthquake damage, as illustrated in Appendix B.

Table 1: Prior distributions for the parameters $\boldsymbol{\vartheta}$ and corresponding means and the 5% and 95% quantiles ($q_{0.05}$ and $q_{0.95}$).

Parameter	Domain	Distribution	Mean	$q_{0.05}$	$q_{0.95}$
β	$\mathbb{R}^+$	$p(\beta) = \text{InvGamma}(\alpha = 2.5, \beta = 1.0)$	0.77	0.20	2.00
η_1	$\mathbb{R}$	$p(\eta_1) = \mathcal{N}(\mu = -1.61, \sigma = 1.5)$	-1.61	-4.08	0.86
$\delta_{ds}\ \forall\, ds > 1$	$\mathbb{R}^+$	$p(\delta_{ds}) = \text{Gamma}(\alpha = 1.5, \beta = 2.5)$	0.6	0.07	1.56

The posterior distribution in Eq. (5) is not analytically tractable, thus we use Markov Chain Monte Carlo (MCMC) sampling for Bayesian inference. MCMC is a computational technique used to approximate complex probability distributions. It combines principles from

Markov chains and Monte Carlo methods to efficiently sample from a target distribution when direct sampling is not feasible. This makes it particularly valuable for Bayesian statistics, where we aim to draw samples from a certain target posterior. Here, we employ the No-U-Turn Sampler (Hoffman and Gelman, 2014) as implemented in the software library NumPyro (Phan et al., 2019). We obtain 3,000 sample sets $(\boldsymbol{\vartheta}, \mathbf{im}_{\mathcal{B}})$ from the posterior through four independent MCMC chains with 1,000 warm-up steps each. The convergence of the chains is tested by following the recommendations of Vehtari et al. (2021) summarized in Appendix C. The implementation details can be found in the provided code repository[1].

Figure 3 illustrates the posterior samples of $(\boldsymbol{\vartheta}, \mathbf{im}_{\mathcal{B}})$, obtained from MCMC, for the same one-dimensional example used in Figure 2. From Figure 3b, we observe how the consideration of the damage survey data allows for an improved estimate on $\mathbf{im}_{\mathcal{B}}$ compared to the case in Figure 2b that uses solely the available station data. Figure 3c plots the fragility functions obtained from the mean of the sampled parameters (dashed lines, corresponding to 0.65, 0.19g, and 0.61g for β, θ_1 and θ_2, respectively), which closely match the "true" data-generating functions. The shaded areas indicate the 90% credibility interval (CI). The latter is the difference between the 95% and 5% quantiles obtained at each im level for all functions computed from the posterior parameter samples. The limited amount of data considered in this simplified example results in relatively large CIs, especially for $ds = 2$.

Accounting for different building characteristics

So far, we have assumed identical fragility functions for all considered buildings. To reflect the heterogeneity in realistic building stocks, the model should account for the differences in structural types, geometry, and other building characteristics. For this purpose, most current regional earthquake risk models use multiple fragility models, each defined for a specific combination of building characteristics. These combinations are here referred to as

[1] www.doi.org/10.5281/zenodo.10074233

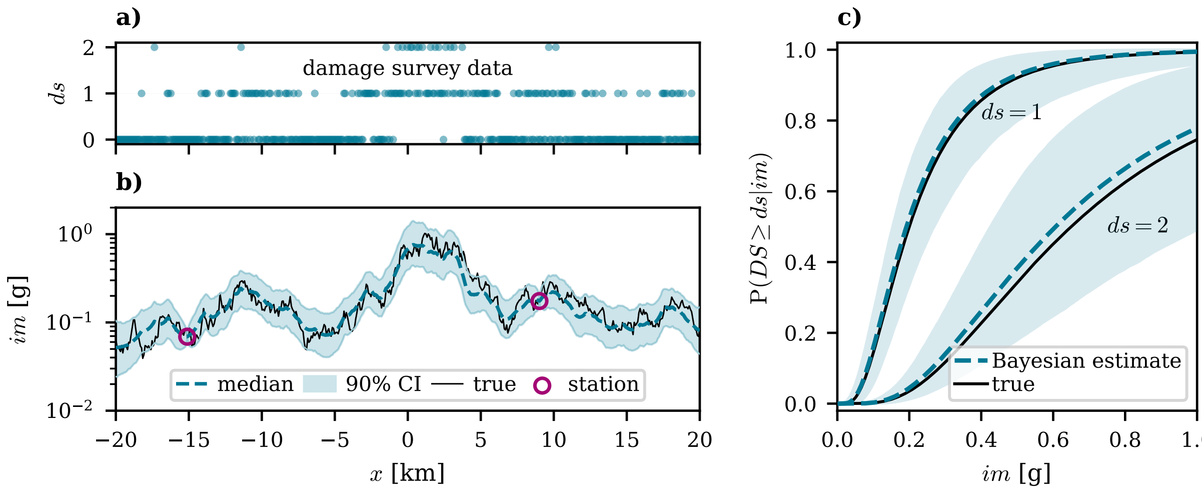

Figure 3: Fragility results from the Bayesian approach for the example from Figure 2: (a) Simulated building damage states plotted versus their location. (b) Simulated "true" *IM* values, with circles denoting the locations and *IM* values for two recording stations. The dashed line and the shaded area indicate the median and the 90% CI of the posterior *IM* distribution conditional on station and damage data. (c) The "true" and the estimated fragility functions. The dashed lines show the functions obtained from the mean posterior parameters, and the shaded area indicates the 90% CI.

building classes and denoted with variable $bc \in \mathcal{BC}$, where $\mathcal{BC}$ is the set of all considered building classes.

The fragility functions for different bc are commonly assumed to be of the same functional form, i.e., the model specified in Eq. (3), but with differing parameters. Thus, the total set of parameters is $\boldsymbol{\vartheta} = \{\boldsymbol{\vartheta}_{bc} | bc \in \mathcal{BC}\}$. When using the fixed *IM* approach, the parameters $\boldsymbol{\vartheta}_{bc}$ are estimated independently for each bc. Thus, it may be necessary to use fewer building classes such that a sufficiently large number of observations per class is available. The proposed Bayesian approach jointly estimates the posterior of *IM* values and all parameters $\boldsymbol{\vartheta}$. This results in a more complex estimation step, but has the advantage that even classes with few observations profit from the reduced uncertainty in the *IM* posterior obtained from all observations.

Information on building characteristics is gathered during the building inspection for post-earthquake damage assessment. The herein presented case study makes use of existing studies that defined a set of building classes, $\mathcal{BC}$. In the general case, however, the choice of $\mathcal{BC}$ and the fragility modeling are inherently connected. It often requires an iterative procedure to check which $\mathcal{BC}$ performs best in distinguishing susceptibility of a building to earthquake damage, while still providing enough observations per building class.

CASE STUDY: THE 2009 L'AQUILA (ITALY) EARTHQUAKE

This case study estimates fragility function parameters using data from the 2009 M6 L'Aquila earthquake. The objectives are twofold: first, to apply the proposed Bayesian estimation method on a real data set and second, to examine the role of IM uncertainty by comparing the Bayesian estimation results to results from the traditional, fixed IM approach. The data set contains results of visual post-earthquake inspections of residential buildings and was published by the Italian civil protection department (Dolce et al., 2019). As such, it provides information on the sustained damage and descriptions of the building characteristics (e.g., the geometry and the structural type). This survey data is combined with rupture characteristics and station data from the engineering strong motion database (Luzi et al., 2020). Figure 4a shows the surface projection of the rupture and the stations located within the region of interest together with soil conditions in terms of the 30 m time-averaged shear-wave velocity, v_{s30}, obtained from Mori et al. (2020).

The considered data set consists of 56,400 masonry buildings distributed over 62 municipalities, as shown in Figure 4b. The damage states are derived from the raw inspection results based on Table 1 in Rosti et al. (2021) and consist of six categories: no ($ds = 0$), negligible to slight ($ds = 1$), moderate ($ds = 2$), severe ($ds = 3$), very heavy damage ($ds = 4$) and collapse ($ds = 5$). In accordance with the national Italian risk assessment (Dolce et al., 2021), we categorize the masonry buildings into three structural types, A, B and C1, with

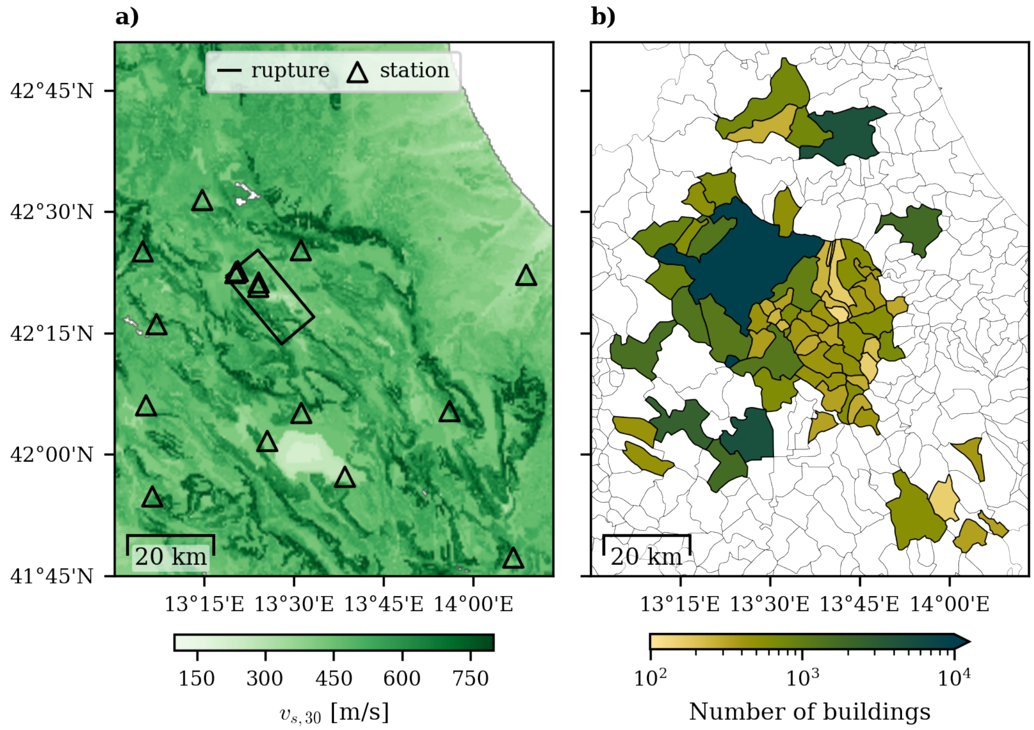

Figure 4: Overview of the L'Aquila case study region: a) seismic network stations, projected rupture surface, and soil conditions as measured via $v_{s,30}$; b) number of buildings per municipality in the considered data set.

decreasing susceptibility to earthquake-induced damage. The link between specific attributes in the damage survey and the three structural types are described in Table 10 in Dolce et al. (2019). Finally, fragility parameters are estimated for six building classes, derived from the structural type and the number of storeys. Specifically, each type is further divided into low-rise structures (less than two storeys) and mid-/high-rise structures (more than three storeys), denoted as L and MH, respectively. We estimate six parameters for each building class, leading to a total of 36 parameters.

The above-described data set was obtained after several pre-processing steps of the raw post-earthquake survey results. One often-encountered challenge in empirical fragility modelling is the under-representation of undamaged buildings. This occurs because inspections may focus preferentially on damaged buildings. To alleviate this issue, we broadly follow the approach taken by Rosti et al. (2021). For each municipality, the number of buildings in the database is compared to statistics from the 2001 national census (ISTAT, 2001). Municipalities where the available data set covers at least 90% of the number of buildings indicated in the census statistics are considered as completely surveyed. For municipalities where this ratio is less than 10%, it is assumed that only damaged buildings were inspected, and the remaining buildings are added to the inspection data set assuming that they are undamaged. Inspection results from municipalities with ratios between 10% and 90% are not considered, due to the challenge of inferring the condition of non-inspected buildings in those cases.

Missing fields in the original inspection data set and the added undamaged buildings result in some buildings having unknown spatial coordinates, number of storeys, or structural type. Buildings with identical or missing coordinates (e.g., the added buildings) are re-distributed based on the European settlement map (Corbane and Sabo, 2019). Missing entries on storey number and structural type are imputed based on census and survey data. For this illustrative case study, we consider the derived inputs as fixed, but we could also propagate such input uncertainty within the proposed Bayesian framework. Of the 56,400 masonry buildings in the final data set, 35,700 (63%) stem from the post-earthquake inspection data set and 20,700 (27%) undamaged buildings are added based on census data. For each considered building class, Table 2 shows the number of buildings per damage state.

Table 2: Number of buildings of a certain building class and damage state for the compiled damage survey data set.

building class	$ds = 0$	$ds = 1$	$ds = 2$	$ds = 3$	$ds = 4$	$ds = 5$
A-L	8,915	2,771	1,219	1,855	2,059	1,570
A-MH	4,633	1,895	810	1,138	1,453	874
B-L	8,763	1,725	494	570	491	352
B-MH	4,871	1,263	377	430	444	290
C1-L	3,425	542	111	107	115	60
C1-MH	2,077	400	93	97	66	55

The pre-processed damage data set, summarized in Table 2, is then used to estimate fragility functions using two approaches: the fixed *IM* approach and the proposed Bayesian, MCMC-based, approach. The latter uses the entire conditional distribution $p(\mathbf{im}_{\mathcal{B}}|\mathbf{im}_{\mathcal{S}}, \mathbf{rup})$, which requires the storage of the $(n \times n)$-dimensional matrix $\mathbf{\Sigma}_{\mathcal{BB}|\mathcal{S}}$. Due to this high memory demand, the size of the considered data set has to be limited. The inference is run on an NVIDIA V100 tensor core GPU with 25 GB of RAM that allows the consideration of data from n =14,000 buildings, corresponding to one fourth of the data set. The data subset is developed by randomly sampling 25% of the buildings from each building class/damage state combination shown in Table 2. For the computationally less expensive fixed *IM* approach, we use the entire data set.

We first estimate fragility functions using $SA(0.3s)$ as the IM. Thus, the vectors $\mathbf{im}_{\mathcal{B}}$ and $\mathbf{im}_{\mathcal{S}}$ are spectral accelerations at sites of surveyed buildings and network stations, respectively. To compute the conditional distribution $p(\mathbf{im}_{\mathcal{B}}|\mathbf{im}_{\mathcal{S}}, \mathbf{rup})$, we use the OpenQuake (Silva et al., 2014) implementation of the Bindi et al. (2011) GMM and the spatial correlation model of Esposito and Iervolino (2012). Figure 5a plots the median spectral accelerations conditional on station data $\mathbf{im}_{\mathcal{S}}$. Recall that this median value is used to estimate parameters $\boldsymbol{\vartheta}$ with the fixed *IM* approach. The Bayesian approach, on the other hand, provides samples from the joint posterior of $\mathbf{im}_{\mathcal{B}}$ and $\boldsymbol{\vartheta}$. The median of the posterior $\mathbf{im}_{\mathcal{B}}$ samples is plotted in Figure 5b, where the locations of the considered buildings are also indicated. We observe that the resulting spatial *IM* pattern is more refined compared to the original map in panel a.

Figure 6 plots the fragility functions of two building classes, A-MH and C1-L, as obtained with the fixed *IM* approach and the proposed Bayesian approach. Similar to the one-dimensional example in Figure 2, we observe that the fixed *IM* based parameter estimates lead to flatter fragility functions compared to those obtained from the Bayesian approach, providing higher damage probabilities for low *IM* values and lower probabilities for large

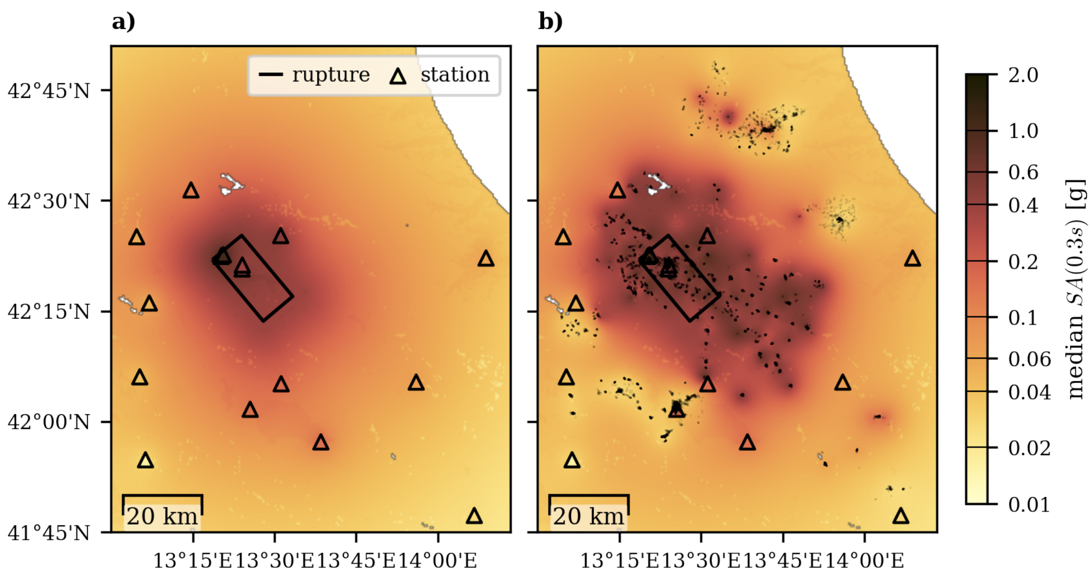

Figure 5: The spatial distribution of median $SA(0.3s)$ values conditional on seismic network recordings (a) and additionally conditioned on damage survey data via the proposed Bayesian approach (b). Network stations and locations of surveyed buildings are indicated with triangles and points, respectively.

IM values. For example, considering building class A-MH in Figure 6a, and a spectral acceleration $SA(0.3s) = 0.25$g, the fragility functions obtained from the fixed IM approach predict a 30% probability of reaching or exceeding $ds = 4$, while this probability decreases to 5% if the mean of the posterior samples is used. For the Bayesian approach, we also note the decrease in the 90% CI compared to the one-dimensional example in Figure 3. This is due to the larger size of the considered damage survey data set, combined with a larger number of seismic stations.

Table 3 provides the estimated fragility function parameters for the six considered building classes. The fixed IM approach leads to substantially larger estimates of the dispersion parameter β, explaining the flatter fragility functions in Figure 6. By fixing IM values to the best-estimate values plotted in Figure 5a, the variability of the actual, unobserved, IM values around these best-estimates manifests in apparent dispersion in the estimated fragility functions, as reflected by the large β values. Both estimation approaches capture the in-

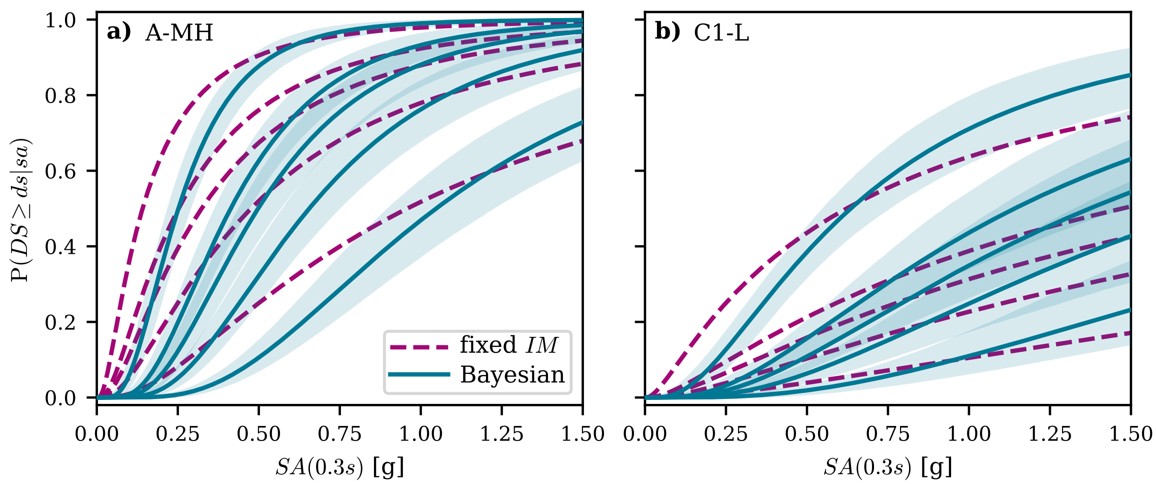

Figure 6: Fragility functions for building class A-MH (a) and C1-L (b) estimated from the damage survey data using the fixed IM and the Bayesian approaches. The five functions correspond to $ds \in \{1, 2, \ldots, 5\}$ from the top left to the bottom right. Functions from the Bayesian approach are illustrated using the mean posterior samples (solid lines) and the 90% CI (shaded area).

creasing damage susceptibility expected from the employed building categorization scheme, i.e., buildings of type A having lower θ_{ds} values and thus being more fragile than buildings of type C1. Furthermore, low-rise buildings (e.g., A-L) tend to be less fragile than their counterparts with more than two storeys (e.g., A-MH).

Table 3: Fragility function parameters for the six considered building classes estimated with the fixed IM approach (FA) and the proposed Bayesian approach (BA). The stated Bayesian parameter estimates correspond to the mean of the posterior samples.

Class	β [-]		θ_1 [g]		θ_2 [g]		θ_3 [g]		θ_4 [g]		θ_5 [g]	
	FA	BA	FA	BA	FA	BA	FA	BA	FA	BA	FA	BA
A-L	1.09	0.68	0.18	0.30	0.31	0.46	0.39	0.55	0.60	0.73	1.13	1.13
A-MH	0.96	0.59	0.14	0.25	0.25	0.41	0.32	0.50	0.48	0.66	0.96	1.05
B-L	1.20	0.81	0.39	0.47	0.78	0.82	1.01	0.99	1.50	1.33	2.65	2.00
B-MH	1.20	0.75	0.29	0.37	0.60	0.65	0.78	0.79	1.15	1.05	2.19	1.62
C1-L	1.35	0.82	0.62	0.63	1.47	1.14	1.93	1.37	2.76	1.74	5.43	2.73
C1-MH	1.17	0.75	0.46	0.52	1.03	0.93	1.35	1.13	2.01	1.49	3.16	2.01

Results using alternate IMs

Only few empirical fragility functions are derived for spectral accelerations, while the majority are based on PGA. The use of $SA(0.3s)$ above was motivated by the fact that it is seen as a more efficient predictor of building response. Given this assumption, we would expect smaller dispersion values, β, when using spectral accelerations. Figure 7 shows the β values estimated for both IMs using the fixed IM and the Bayesian approaches. Indeed, the β values for $SA(0.3s)$ are slightly smaller for both approaches. The small difference may be explained by the fact that we focus on masonry buildings that are almost all less than four storeys tall, thus representing relatively heavy and non-ductile structures for which PGA can be an adequate fragility predictor. For the remainder of this study, we continue with $SA(0.3s)$ as the IM of interest.

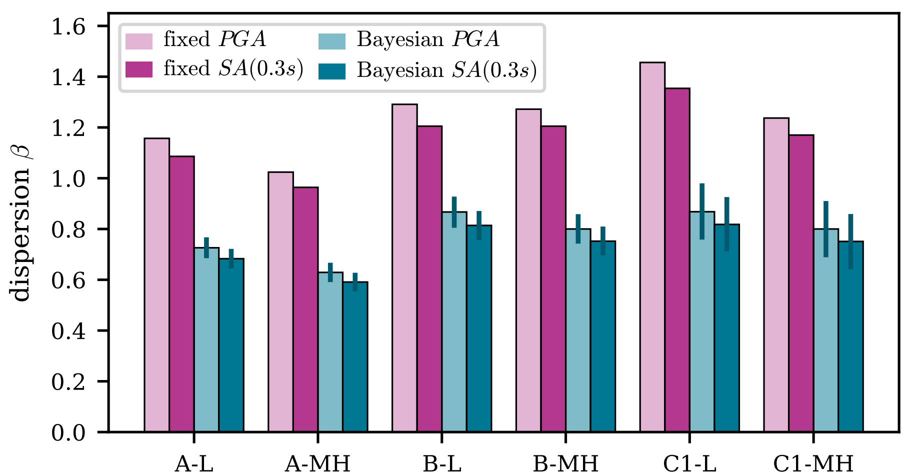

Figure 7: Comparison of estimated β values from the fixed IM and the Bayesian approach for PGA and $SA(0.3s)$.

Comparison for different GMMs

So far, we used the Bindi et al. (2011) GMM and the Esposito and Iervolino (2012) correlation model to establish the distribution of IM values conditional on station data (illustrated by its median in Figure 5a). These models are calibrated on Italian ground motion data and used in the official Italian shake map system (Michelini et al., 2020). We denote this combination as GMM1. Here, we will compare the parameter estimates obtained with GMM1 to the ones resulting from a second combination, named GMM2, that uses the Chiou and Youngs (2014) GMM and the correlation model of Bodenmann et al. (2023). Both GMM2 models are estimated on the same global ground motion data set. The change of input motion models affects only the $\mathbf{im}_{\mathcal{B}}$ distribution in Figure 1, and we use the alternate distribution to then re-estimate the fragility parameters, $\boldsymbol{\vartheta}$.

Figure 8 shows the fragility functions for A-L buildings derived using GMM1 and GMM2, respectively. For better readability, only the mean Bayesian estimates are shown. From Figure 8b we observe that the functions obtained from the Bayesian approach are similar for both GMMs, while Figure 8a indicates a substantial sensitivity on the underlying GMM for the fixed IM approach. In the latter case, the parameter estimates based on GMM2 indicate less fragile buildings. The reasons for these differences are explained below.

The alternate models within GMM1 and GMM2 predict differing $SA(0.3s)$ values for the rupture due to differences in functional forms, dependent variables, and the data used in fitting the models' parameters. To illustrate these differences, we compare the $SA(0.3s)$ predictions along the horizontal transect illustrated in Figure 9a. Figure 9b plots the predictive distributions in terms of the median and the 90% CI, prior to taking into account station recordings and damage survey data. For sites located within the rupture surface projection, GMM2 predicts larger $SA(0.3s)$ values than GMM1. These differences also persist after taking into account station recordings, as visible from the corresponding distributions in

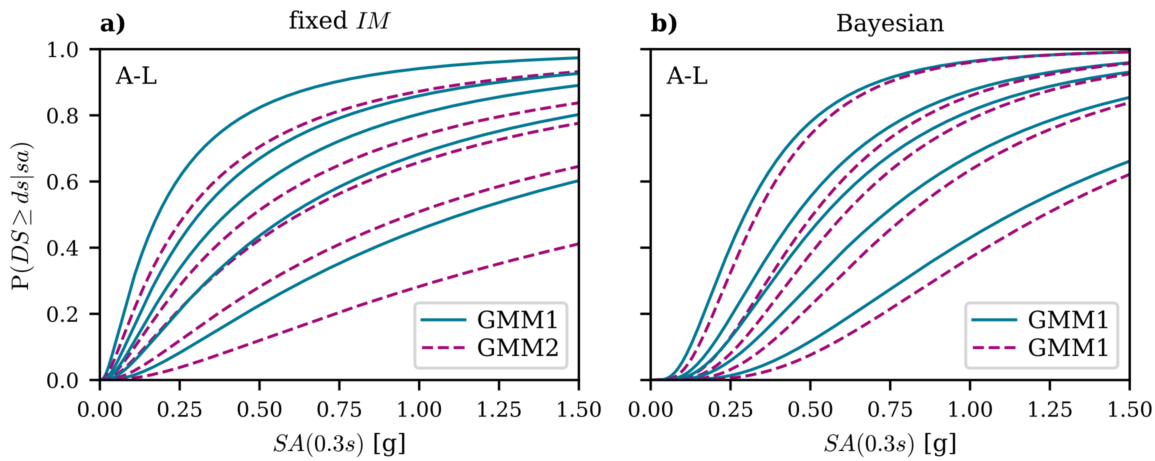

Figure 8: Comparison of fragility functions for building class A-L that are estimated using two different combinations of ground motion and spatial correlation models (GMM1 and GMM2) through the fixed IM approach (a) and the proposed Bayesian approach (b).

Figure 9c. Recall that the fixed IM approach uses the median values indicated in Figure 9c to estimate the fragility functions. This explains the differences in the estimated functions discussed above and shown in Figure 8a.

Finally, Figure 9d plots the distributions as obtained after processing the damage data through the proposed Bayesian approach. For locations in the vicinity of surveyed buildings, we observe similar distributions from both GMMs. By performing joint Bayesian inference over $SA(0.3s)$ values and fragility parameters, the posterior $SA(0.3s)$ distributions tend to converge regardless of whether GMM1 or GMM2 is used to establish the prior distribution of $SA(0.3s)$ values. This explains the similarity in the estimated fragility functions observed in Figure 8b, and indicates that the proposed Bayesian approach is more robust than the traditional, fixed IM, approach with respect to such modelling assumptions.

Effect of data sub-sampling

The proposed Bayesian approach is computationally expensive, and thus only one fourth of the entire data set is used for parameter estimation. This is a drawback compared to

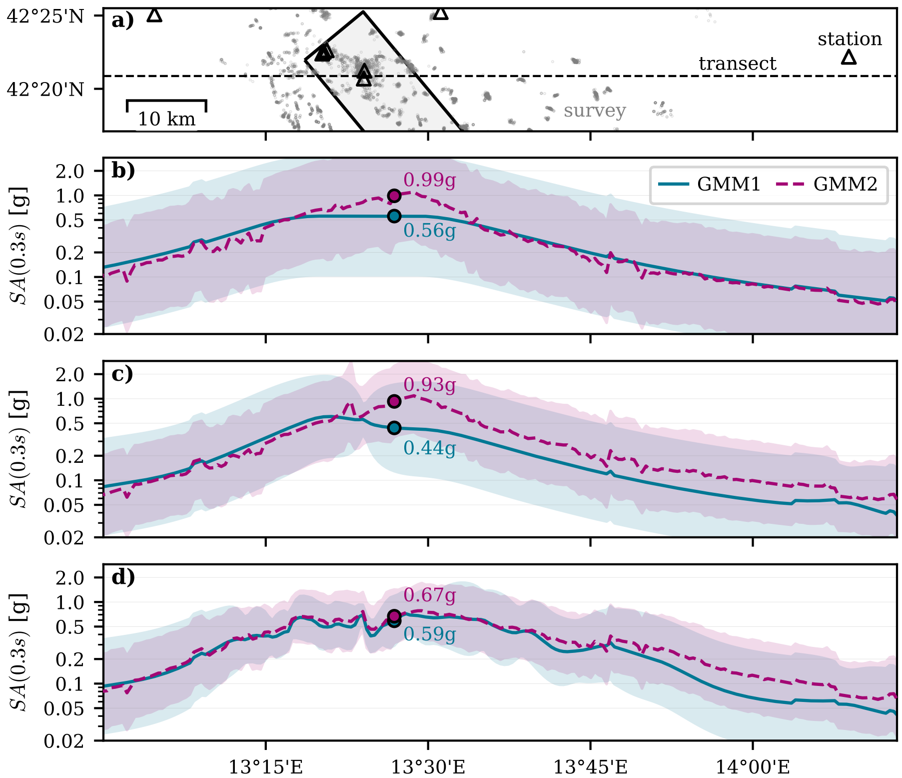

Figure 9: Comparison of $SA(0.3s)$ median values and 90% CIs obtained from GMM1 and GMM2, and plotted along a horizontal transect through the region: (a) Stations and surveyed buildings in the vicinity of the chosen transect. (b) GMM predictions conditional on rupture characteristics; (c) after additional conditioning on station data; and (d) after additional conditioning on damage data using the Bayesian approach. The labeled points in (b to d) are example values for a numerical comparison.

the fixed IM approach that handles the entire data set with no computational difficulties, and raises the question of how the Bayesian parameter estimates change for different subsets. Figure 10 shows β values estimated with four randomly chosen sub-samples of the entire data set. The four estimated values for each building class are within the posterior distribution CIs, and with differences that are much less than the difference relative to the fixed IM values, indicating that the proposed approach produces stable outputs even with random sub-sampling. This is perhaps not surprising given the large number of observations that remain within a given sub-sample. Recall that we randomly selected 25% of the data points from each building class/damage state combination shown in Table 2. The use of more sophisticated sub-sampling techniques is likely to further reduce the sensitivity of the estimated parameters.

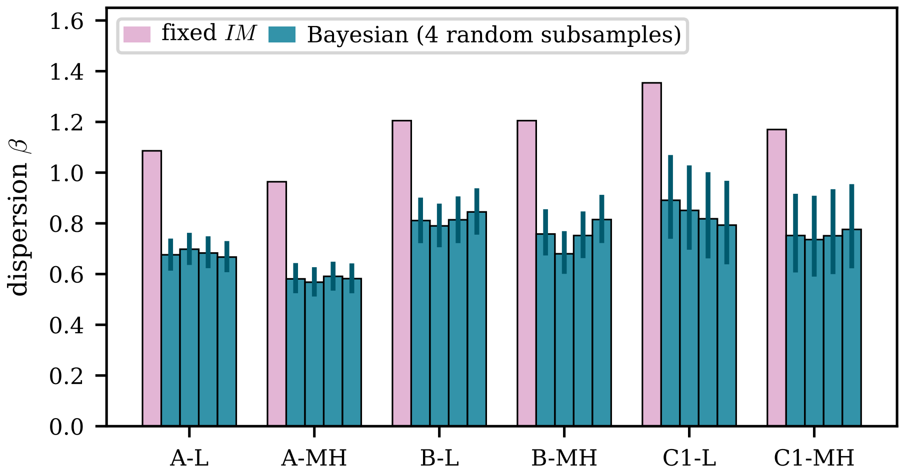

Figure 10: Comparison of estimated β values from the fixed *IM* approach and for MCMC estimated from four random subsamples of the entire data set.

In a separate analysis, we compare the performance of both estimation methods in recovering a set of known, "true", fragility functions while using the same sub-sampling technique as above. For this purpose, we replace the observed damage states in the L'Aquila data set by simulated values. These are obtained by first drawing one sample of $\mathbf{im}_{\mathcal{B}}$ from the established conditional distribution $p(\mathbf{im}_{\mathcal{B}}|\mathbf{im}_{\mathcal{S}}, \mathbf{rup})$ and then using a pre-defined set of fragility functions to sample a damage state for each building. Figure 11 compares the estimated fragility functions of two building classes, A-L and B-MH, to the "true" data-generating functions. For better readability, we only plot the functions for $ds \in \{1, 2, 4\}$. The functions obtained from the fixed *IM* approach are flatter than the "true" functions, while the Bayesian approach leads to functions that are in good agreement, despite only one fourth of the data set being used.

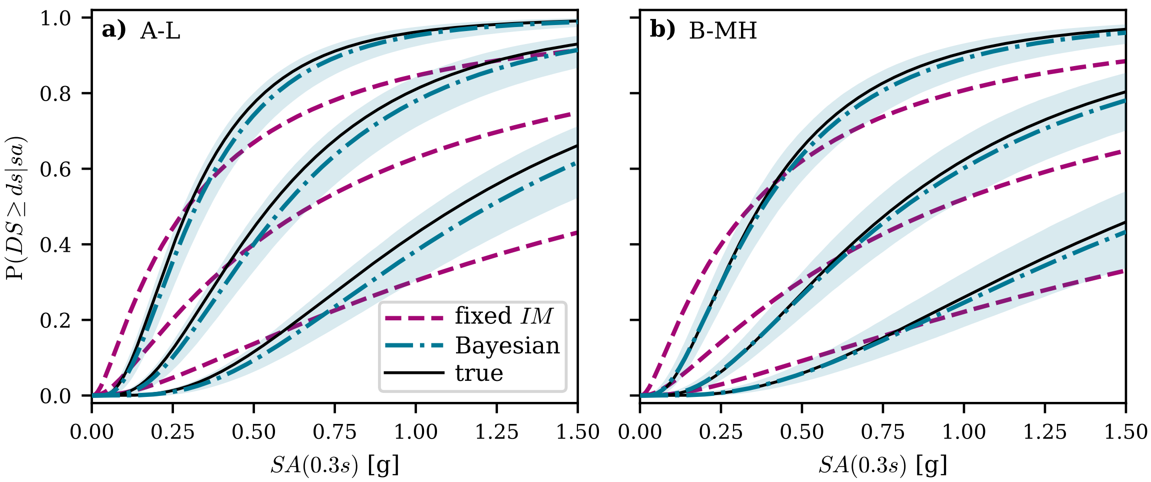

Figure 11: Comparison of fragility functions of building class A-L (a) and B-MH (b) estimated from a simulated version of the L'Aquila damage survey data set to the "true" data-generating functions. For better readability, only functions for $ds \in \{1, 2, 4\}$ are plotted (from top left to bottom right).

CONCLUSION

This study explored the role of IM uncertainty in the estimation of fragility function parameters from damage survey data gathered after earthquake events, and proposed a novel estimation method that can account for this uncertainty. Traditional estimation methods do not allow to account for such uncertainty and instead assume fixed, deterministic, IM values. In simulated case studies, traditional methods reportedly failed to recover the "true" data-generating fragility functions. To address this shortcoming, we proposed a Bayesian estimation approach that simultaneously considers IM values and fragility function parameters as uncertain variables. We derived an expression for their joint distribution conditional on the gathered damage data. For parameter estimation, we approximate this posterior distribution through MCMC sampling.

We applied the proposed method in a case study using damage data gathered after the 2009 L'Aquila earthquake event. The data set consists of 56,400 residential masonry buildings that are categorized into six building classes and for which overall damage is described with six categories ranging from no damage to collapse.

We used both synthetic data and the L'Aquila data to compare the Bayesian parameter estimates with estimates from a traditional, fixed IM, approach. The two methods produce surprisingly different fragility functions, with those obtained from the fixed IM approach being flatter than their counterparts derived with the proposed Bayesian approach. The flatter fragility functions predict higher probabilities of damage for low IM values and, conversely, lower probabilities for high IM values. Such behavior is observed across all damage states and building classes. By fixing IM values to best-estimate values, the variability of the actual, unobserved, IM values around these best-estimates manifests in an increased apparent dispersion in the estimated fragility functions. The proposed Bayesian approach, on the other hand, explicitly accounts for both variability sources and performs joint inference on IM values and model parameters, which prevents such an inflation of fragility function dispersion.

Additional tests demonstrated that the proposed Bayesian approach is less sensitive to the choice of ground motion and spatial correlation models used to derive the distribution of IM conditional on station data (i.e., the shake map) than the traditionally used method, which relies on fixed IM values. This reduced sensitivity is a significant advantage, as the IM predictions from any given ground motion and spatial correlation model are not "correct", as must be assumed with the fixed IM method. The proposed method of jointly estimating the IM values and fragility parameters allows for more robust estimates with respect to such modeling assumptions.

The proposed Bayesian approach comes with computational challenges, in particular with respect to memory demand. The herein used implementation could perform inference for 14,000 data points. This number is sufficient for many damage data sets, but its application to the L'Aquila data set required sub-sampling the data set. To assess the implications of such sub-sampling we performed two analyses. First, we found that the parameters estimated from multiple randomly chosen subsets were relatively stable across the different subsets. Second, we replaced the observed damage with simulated values and found that the Bayesian approach could recover the "true" data-generating fragility functions using only a subset of the data. The fixed *IM* approach, on the other hand, failed to do so even when the entire data set was used for parameter estimation. While the proposed method does require an additional analyst effort and more computational resources relative to the traditional estimation method, the required effort is still vastly smaller than the time and cost of inspections to collect the damage data, and so is a good investment given the extra value it provides.

While the focus of the presented work lies on *IM* uncertainty, the proposed method can be extended to account for uncertainties in other model inputs, such as missing database entries. The method could also be adapted to fragility models that have different dispersion parameters for each damage level and depend on building characteristics in a more complex manner than the commonly used categorization into pre-defined building classes. Despite these opportunities for further research, the novel estimation method can already be of substantial benefit for analysts interested in improved empirical fragility modeling. For the above reasons, we strongly believe that the method's presented comparative advantages justify its increased computational complexity.

Software tool To facilitate the application of the proposed Bayesian parameter estimation approach, we developed a user-friendly Python-based software tool, which is available at www.doi.org/10.5281/zenodo.10074233. The tool comes with several tutorials and example data sets that further explain the features and implementations of the proposed estimation procedure. Importantly, it contains the code to reproduce the herein presented results and figures.

Acknowledgements The first author gratefully acknowledges support from the ETH Risk Center (grant 2018-FE-213).

APPENDIX

A DISTRIBUTION OF IM VALUES CONDITIONAL ON STATION DATA

This appendix provides further details on the approach of Engler et al. (2022) that was used in this study to compute the distribution of IM values at locations of surveyed buildings, $\mathbf{im}_{\mathcal{B}}$, conditional on IM values at locations of seismic network stations, $\mathbf{im}_{\mathcal{S}}$, and rupture characteristics $\mathbf{rup}$. For this purpose, we first look at the distribution of IM values at a generic set of spatially distributed sites conditional on $\mathbf{rup}$ and in absence of station data. These values are assumed to follow a multivariate log-normal distribution (Jayaram and Baker, 2008), in other words the $\ln IM$ values follow a multivariate normal distribution with mean vector $\boldsymbol{\mu}$ and covariance matrix $\boldsymbol{\Sigma}$. For each site i, empirical GMMs allow computing the mean, μ_i, of $\ln IM_i$ and the standard deviations, τ_i and ϕ_i, of the between- and within-event residual, respectively. The between-event residual is constant for any two sites i and j, while the within-event residuals are partially correlated with coefficient ρ_{ij}. The latter is computed with a spatial correlation model. The entries of the covariance matrix are $[\boldsymbol{\Sigma}]_{ij} = \tau_i\tau_j + \phi_i\phi_j\rho_{ij}$, while the entries of the mean vector $\boldsymbol{\mu}$ follow from the predicted mean values μ_i obtained from the GMM. Thus, the joint distribution of IM values at survey and station sites is a multivariate log-normal distribution expressed as

$$p\left(\begin{bmatrix}\mathbf{im}_{\mathcal{B}}\\ \mathbf{im}_{\mathcal{S}}\end{bmatrix} \mid \mathbf{rup}\right) = \mathcal{LN}\left(\begin{bmatrix}\boldsymbol{\mu}_{\mathcal{B}}\\ \boldsymbol{\mu}_{\mathcal{S}}\end{bmatrix}; \begin{bmatrix}\boldsymbol{\Sigma}_{\mathcal{BB}} & \boldsymbol{\Sigma}_{\mathcal{BS}}\\ \boldsymbol{\Sigma}_{\mathcal{SB}} & \boldsymbol{\Sigma}_{\mathcal{SS}}\end{bmatrix}\right) , \tag{A1}$$

where $\boldsymbol{\mu}_{\mathcal{B}}$ and $\boldsymbol{\Sigma}_{\mathcal{BB}}$ denote the mean vectors and covariance matrices of $\ln IM$ values at the locations of the surveyed buildings, $\boldsymbol{\mu}_{\mathcal{S}}$ and $\boldsymbol{\Sigma}_{\mathcal{SS}}$ their counterparts at the station locations, and $\boldsymbol{\Sigma}_{\mathcal{BS}}$ the covariance matrix between the $\ln IM$ values at the buildings and the stations. Then, the parameters of $p(\mathbf{im}_{\mathcal{B}}|\mathbf{im}_{\mathcal{S}}, \mathbf{rup})$ follow as

$$\boldsymbol{\mu}_{\mathcal{B}|\mathcal{S}} = \boldsymbol{\mu}_{\mathcal{B}} + \boldsymbol{\Sigma}_{\mathcal{BS}}\boldsymbol{\Sigma}_{\mathcal{SS}}^{-1}(\ln \mathbf{im}_{\mathcal{S}} - \boldsymbol{\mu}_{\mathcal{S}}) \tag{A2a}$$

$$\boldsymbol{\Sigma}_{\mathcal{BB}|\mathcal{S}} = \boldsymbol{\Sigma}_{\mathcal{BB}} - \boldsymbol{\Sigma}_{\mathcal{BS}}\boldsymbol{\Sigma}_{\mathcal{SS}}^{-1}\boldsymbol{\Sigma}_{\mathcal{SB}} \ , \tag{A2b}$$

where $\boldsymbol{\mu}_{\mathcal{B}|\mathcal{S}}$ and $\boldsymbol{\Sigma}_{\mathcal{BB}|\mathcal{S}}$ denote the mean vector and covariance matrix of $\ln IM$ values at the surveyed buildings conditional on station data $\mathbf{im}_{\mathcal{S}}$.

B PRIOR DISTRIBUTION OF FRAGILITY FUNCTION PARAMETERS

Figure B1 illustrates the prior distributions for the fragility function parameters $\boldsymbol{\vartheta}$ stated in Table 1 and plots the fragility functions obtained from these priors using an example of three damage states, where $\boldsymbol{\vartheta} = (\beta, \eta_1, \delta_2)$. For each $\boldsymbol{\vartheta}$, the fragility functions are obtained by computing $\eta_2 = \eta_1 + \delta_2$, and Eq. (3). Alternatively, we may compute the median IM which causes the structure to reach or exceed ds as $\theta_{ds} = \exp(\beta\eta_{ds})$, and then use Eq. (1).

C MCMC CONVERGENCE DIAGNOSTICS

This appendix provides a brief summary on the conducted tests to verify the convergence of the target distribution samples obtained from Markov Chain Monte Carlo (MCMC) simulations. Sequences of iterative simulations can fail to converge, either because the chains are in different parts of the target distribution or because the chains have not attained stationarity. Thus, it is crucial to run multiple independent chains for convergence diagnostics. As a first visual convergence assessment, one may compare the distribution of posterior samples from each chain, as well as their sample traces. In the presented case study, we performed MCMC over 14,036 variables (36 damage model parameters and the IMs at 14,000 sites). Performing a visual assessment for each single variable is not practicable for such high-dimensional exer-

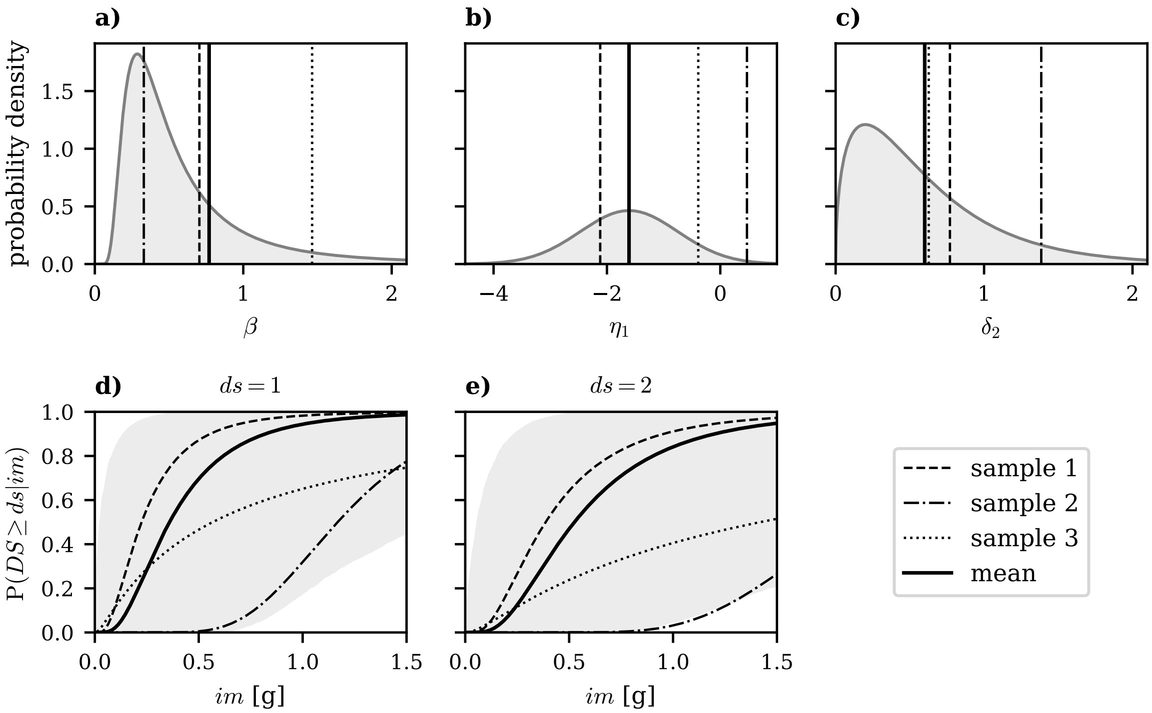

Figure B1: Illustration of the prior distributions for fragility function parameters β, η_1, δ_2 (a to c), and of the fragility functions obtained from the prior mean parameters, as well as three sampled parameter sets, for: d) $ds = 1$, and e) $ds = 2$.

cises. In such cases, we analyze quantitative metrics that indicate poor convergence and flag potential problems. The conducted diagnostics use information between and within chains and are based on Vehtari et al. (2021) to which an interested reader is referred to for further details. The diagnostic metrics are computed with the Phython-based software library ArviZ (Kumar et al., 2019).

The arguably most popular metric is the potential scale reduction factor, $\hat{R}$, introduced by Gelman and Rubin (1992), which compares the variance between multiple chains to the variance within each chain. If the chains converge, the between-chain and within-chain variances should be identical, i.e., $\hat{R} \approx 1$. In addition to $\hat{R}$, we also compute the effective sample size (ESS) of a quantity of interest. In simple terms, ESS states how many independent draws contain the same amount of information as the dependent sample obtained via MCMC. Both measures, $\hat{R}$ and ESS, are computed based on rank-normalized samples as recommended by Vehtari et al. (2021). Based on the heuristics presented by the same study, good convergence is achieved if $\hat{R} \leq 1.01$ and ESS > 400. Consequently, we chose the number of samples (750 per chain) and warm-up steps (1,000 per chain) such that both of these conditions are fulfilled.

REFERENCES

Baker JW (2015) Efficient Analytical Fragility Function Fitting Using Dynamic Structural Analysis. *Earthquake Spectra* 31(1): 579–599. doi:10.1193/021113EQS025M.

Basöz N and Kiremidjian AS (1998) Evaluation of Bridge Damage Data from the Loma Prieta and Northridge, California Earthquakes. Technical report, The John A. Blume Earthquake Engineering Center, Stanford University, Stanford, California.

Bindi D, Pacor F, Luzi L, Puglia R, Massa M, Ameri G and Paolucci R (2011) Ground motion prediction equations derived from the Italian strong motion database. *Bulletin of Earthquake Engineering* 9(6): 1899–1920. doi:10.1007/s10518-011-9313-z.

Bodenmann L, Baker JW and Stojadinović B (2023) Accounting for path and site effects in spatial ground-motion correlation models using Bayesian inference. *Natural Hazards and Earth System Sciences* 23(7): 2387–2402. doi:10.5194/nhess-23-2387-2023.

Chiou BSJ and Youngs RR (2014) Update of the Chiou and Youngs NGA Model for the Average Horizontal Component of Peak Ground Motion and Response Spectra. *Earthquake Spectra* 30(3): 1117–1153. doi:10.1193/072813EQS219M.

Corbane C and Sabo F (2019) European Settlement Map from Copernicus Very High Resolution data for reference year 2015, Public Release 2019. European commission, joint research centre (jrc). doi:10.2905/8BD2B792-CC33-4C11-AFD1-B8DD60B44F3B.

Dolce M, Prota A, Borzi B, da Porto F, Lagomarsino S, Magenes G, Moroni C, Penna A, Polese M, Speranza E, Verderame GM and Zuccaro G (2021) Seismic risk assessment of residential buildings in Italy. *Bulletin of Earthquake Engineering* 19(8): 2999–3032. doi:10.1007/s10518-020-01009-5.

Dolce M, Speranza E, Giordano F, Borzi B, Bocchi F, Conte C, Meo AD, Faravelli M and Pascale V (2019) Observed damage database of past Italian earthquakes: The Da.D.O. WebGIS. *Bollettino di Geofisica Teorica ed Applicata* 60(2): 141–164. doi:10.4430/bgta0254.

Engler DT, Worden CB, Thompson EM and Jaiswal KS (2022) Partitioning Ground Motion Uncertainty When Conditioned on Station Data. *Bulletin of the Seismological Society of America* 112(2): 1060–1079. doi:10.1785/0120210177.

Esposito S and Iervolino I (2012) Spatial correlation of spectral acceleration in European data. *Bulletin of the Seismological Society of America* 102(6): 2781–2788. doi:10.1785/0120120068.

Gelman A and Rubin DB (1992) Inference from Iterative Simulation Using Multiple Sequences. *Statistical Science* 7(4). doi:10.1214/ss/1177011136.

Hoffman MD and Gelman A (2014) The No-U-Turn sampler: adaptively setting path lengths in Hamiltonian Monte Carlo. *Journal of Machine Learning Research* 15(1): 1593–1623. doi:10.5555/2627435.2638586.

Ioannou I, Douglas J and Rossetto T (2015) Assessing the impact of ground-motion variability and uncertainty on empirical fragility curves. *Soil Dynamics and Earthquake Engineering* 69: 83–92. doi:10.1016/j.soildyn.2014.10.024.

ISTAT (2001) Censimento generale della popolazione e delle abitazioni. Italian national institute of statistics. URL http://dawinci.istat.it/jsp/MD/.

Jayaram N and Baker JW (2008) Statistical Tests of the Joint Distribution of Spectral Acceleration Values. *Bulletin of the Seismological Society of America* 98(5): 2231–2243. doi:10.1785/0120070208.

Kennedy R, Cornell C, Campbell R, Kaplan S and Perla H (1980) Probabilistic seismic safety study of an existing nuclear power plant. *Nuclear Engineering and Design* 59(2): 315–338. doi:10.1016/0029-5493(80)90203-4.

King S, Kiremidjian, A S, Sarabandi P and Pachakis D (2005) Correlation of observed building performance with measured ground motion. Technical report, The John A. Blume Earthquake Engineering Center, Stanford University, Stanford, California.

Kircher CA, Nassar AA, Kustu O and Holmes WT (1997) Development of Building Damage Functions for Earthquake Loss Estimation. *Earthquake Spectra* 13(4): 663–682. doi: 10.1193/1.1585974.

Kumar R, Carroll C, Hartikainen A and Martin O (2019) ArviZ a unified library for exploratory analysis of Bayesian models in Python. *Journal of Open Source Software* 4(33): 1143. doi:10.21105/joss.01143.

Lallemant D, Kiremidjian A and Burton H (2015) Statistical procedures for developing earthquake damage fragility curves. *Earthquake Engineering & Structural Dynamics* 44(9): 1373–1389. doi:10.1002/eqe.2522.

Luzi L, Lanzano G, Felicetta C, D'Amico M, Russo E, Sgobba S, Pacor F and ORFEUS Working Group 5 (2020) Engineering Strong Motion Database (ESM) (Version 2.0). Instituto nazionale di geofisica e vulcanologia (ingv). doi:10.13127/ESM.2.

Martins L and Silva V (2020) Development of a fragility and vulnerability model for global seismic risk analyses. *Bulletin of Earthquake Engineering* doi:10.1007/s10518-020-00885-1.

Michelini A, Faenza L, Lanzano G, Lauciani V, Jozinović D, Puglia R and Luzi L (2020) The New ShakeMap in Italy: Progress and Advances in the Last 10 Yr. *Seismological Research Letters* 91(1): 317–333. doi:10.1785/0220190130.

Mori F, Mendicelli A, Moscatelli M, Romagnoli G, Peronace E and Naso G (2020) A new Vs30 map for Italy based on the seismic microzonation dataset. *Engineering Geology* 275: 105745. doi:10.1016/j.enggeo.2020.105745.

Mosalam KM, Ayala G, White RN and Roth C (1997) Seismic Fragility of LRC Frames with and without Masonry Infill Walls. *Journal of Earthquake Engineering* 1(4): 693–720. doi:10.1080/13632469708962384.

Nguyen M and Lallemant D (2022) Order Matters: The Benefits of Ordinal Fragility Curves for Damage and Loss Estimation. *Risk Analysis* 42(5): 1136–1148. doi:10.1111/risa.13815.

Phan D, Pradhan N and Jankowiak M (2019) Composable effects for flexible and accelerated probabilistic programming in NumPyro. arxiv. doi:10.48550/ARXIV.1912.11554.

Porter K, Kennedy R and Bachman R (2007) Creating Fragility Functions for Performance-Based Earthquake Engineering. *Earthquake Spectra* 23(2): 471–489. doi:10.1193/1.2720892.

Pozzi M and Wang Q (2018) Gaussian Process Regression and Classification for Probabilistic Damage Assessment of Spatially Distributed Systems. *KSCE Journal of Civil Engineering* 22(3): 1016–1026. doi:10.1007/s12205-018-0014-x.

Rojahn C and Sharpe R (1985) ATC 13: Earthquake damage evaluation data for California. Technical report, Applied Technology Council, Redwood City, CA.

Rossetto T and Ioannou I (2018) Empirical Fragility and Vulnerability Assessment: Not

Just a Regression. In: *Risk Modeling for Hazards and Disasters*. Elsevier, pp. 79–103. doi:10.1016/B978-0-12-804071-3.00004-5.

Rossetto T, Ioannou I, Grant DN and Maqsood T (2014) Guidelines for empirical vulnerability assessment. Technical report, GEM Foundation, Pavia, Italy. doi:10.13117/GEM.VULN-MOD.TR2014.11.

Rosti A, Rota M and Penna A (2021) Empirical fragility curves for Italian URM buildings. *Bulletin of Earthquake Engineering* 19(8): 3057–3076. doi:10.1007/s10518-020-00845-9.

Silva V, Crowley H, Pagani M, Monelli D and Pinho R (2014) Development of the OpenQuake engine, the Global Earthquake Model's open-source software for seismic risk assessment. *Natural Hazards* 72(3): 1409–1427. doi:10.1007/s11069-013-0618-x.

Vehtari A, Gelman A, Simpson D, Carpenter B and Bürkner PC (2021) Rank-Normalization, Folding, and Localization: An Improved Rˆ for Assessing Convergence of MCMC (with Discussion). *Bayesian Analysis* 16(2). doi:10.1214/20-BA1221.